Pt/CeO2 as Catalyst for Non-Oxidative Coupling of Methane

THE JOURNAL OF PHYSICAL CHEMISTRY LETTERS
A JOURNAL OF THE AMERICAN CHEMICAL SOCIETY

pubs.acs.org/JPCL

Letter

Pt/CeO_2 as Catalyst for Nonoxidative Coupling of Methane: Oxidative Regeneration

Hao Zhang, Valery Muravev, Liang Liu, Anna Liutkova, Jérôme F. M. Simons, Blanka Detlefs, Huaizhou Yang, Nikolay Kosinov,* and Emiel J. M. Hensen*

Cite This: *J. Phys. Chem. Lett.* 2023, 14, 6778−6783

Read Online

ACCESS | Metrics & More | Article Recommendations | Supporting Information

ABSTRACT: Direct nonoxidative coupling is a promising route for methane upgrading, yet its commercialization is hindered by the lack of efficient catalysts. Pt/CeO_2 catalysts with isolated Pt species have attracted an increasing amount of interest in recent years. Herein, we studied the catalytic role and evolution of isolated Pt centers on CeO_2 prepared by flame spray pyrolysis under the harsh reaction conditions of nonoxidative methane coupling. During the reaction at 800 °C, the isolated Pt sites sinter, leading to a loss of the ethylene and ethane yield. The agglomerated Pt can be redispersed by using an *in situ* regeneration strategy in oxygen. We found that isolated Pt centers are able to activate methane only at the initial reaction stage, and the $CePt_5$ alloy acts as the active phase in the prolonged reaction.

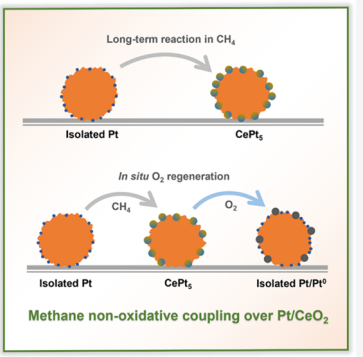

Nonoxidative coupling of methane to more valuable hydrocarbons is a potential route for natural gas and biogas valorization.[1−4] The pioneering study of a highly active and stable Fe©SiO_2 catalyst by Bao and co-workers led to a substantial research effort in this area.[1,5,6] The isolated Fe centers in the Fe©SiO_2 catalyst are argued to limit C−C coupling and, therefore, coke formation on the catalytic surface. Based on this insight, other catalysts containing isolated metal sites such as Pt/CeO_2,[7−11] Pt/C_3N_4,[12] and Ru/TiO_2[13] have been explored for nonoxidative coupling of methane. Xie et al. were the first to report on the use of Pt/CeO_2 with isolated Pt sites for the NOCM reaction.[7] A methane conversion of 14.4% with a C_2-hydrocarbon selectivity of 74.6% was obtained from a 1 vol % CH_4 feed. The authors reported that Pt remained isolated during a 40 h stability test. Later, Bajec et al. used microkinetic analysis of Pt/CeO_2 catalysts with isolated Pt sites to demonstrate that hydrogen abstraction from methane determines the overall rate, while surface C−C coupling reactions only slightly affect the overall CH_4 conversion.[8] Eggart et al. investigated Pt-doped CeO_2 catalysts by *operando* X-ray absorption spectroscopy and synchrotron-based vacuum ultraviolet photoionization mass spectrometry.[11] Methyl radicals were detected as the main reaction intermediate, indicating that gas-phase reactions are involved in the formation of C_2-hydrocarbons. Different from the study by Xie et al.,[7] these authors observed extensive sintering of the initially isolated Pt sites. The agglomeration of Pt was observed even after He treatment at this temperature. The authors also contended that methane activation can occur at the interface between Pt and the ceria support. Theoretical studies have also been carried out to understand the reaction mechanism on such Pt/CeO_2 catalysts. Wen et al. performed a detailed density functional theory (DFT) study, showing that methane conversion strongly depends on the Pt particle size.[9] Isolated Pt on CeO_2 was predicted to exhibit the highest C_2-hydrocarbon selectivity. Chang and co-workers reported that the active sites in Pt/CeO_2 involve two functionalities, namely, single Pt atoms close to a frustrated Lewis acid obtained upon oxygen removal from ceria, which are together involved in methane activation under NOCM conditions.[10] Despite the growing interest in Pt/CeO_2 for the NOCM reaction, it remains unclear how isolated Pt sites behave under harsh reaction conditions.

In the present study, Pt/CeO_2 was prepared by the one-step flame spray pyrolysis (FSP), which is a proven method to synthesize catalysts with highly dispersed metal species.[11,14] Fourier and wavelet transformed EXAFS demonstrates the isolated nature of Pt in which only one clear Pt−O coordination shell at ∼1.6 Å is observed (Figure 1a, Figure S1). XPS analysis shows the predominance of Pt^{2+} species, with a Pt $4f_{7/2}$ binding energy of ∼72.9 eV on the surface of the fresh catalyst (Figure S2). Previous experimental and theoretical studies have supported the interpretation of such

Received: May 1, 2023
Accepted: July 18, 2023
Published: July 21, 2023

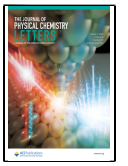

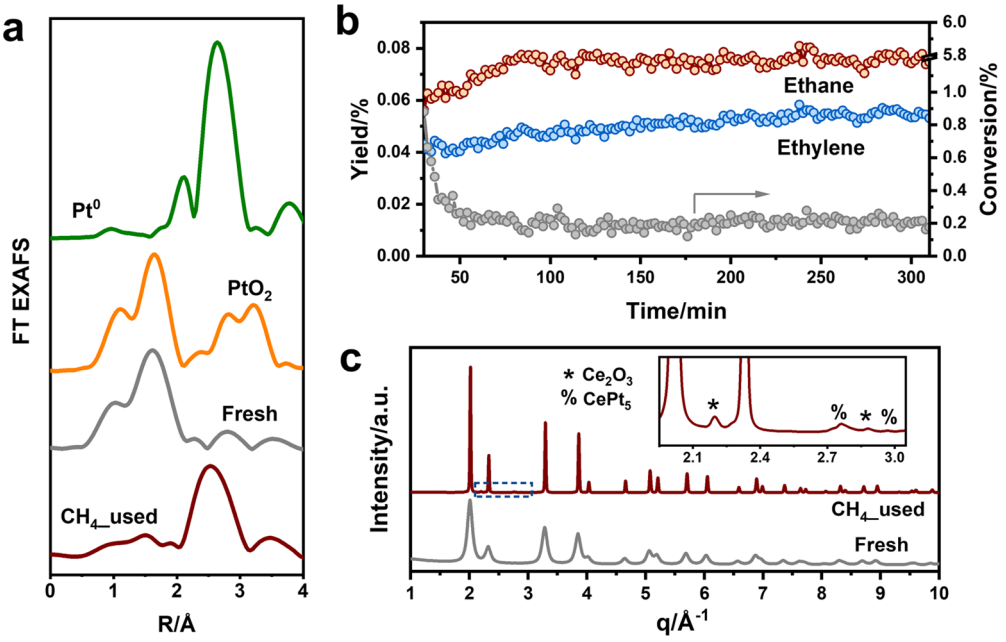

Figure 1. (a) k^3-weighted EXAFS measured at the Pt L_3 edge of fresh and used Pt/CeO_2 catalysts. The Pt^0 and PtO_2 references are included for comparison. (b) Catalytic performance of the Pt/CeO_2 catalyst at 800 °C using 100 mg catalysts under 10 mL/min 95 vol % CH_4 with 5 vol % Ar. (c) Synchrotron XRD patterns of fresh and used Pt/CeO_2 catalysts. The inset shows the enlarged region highlighted by the blue dashed cube.

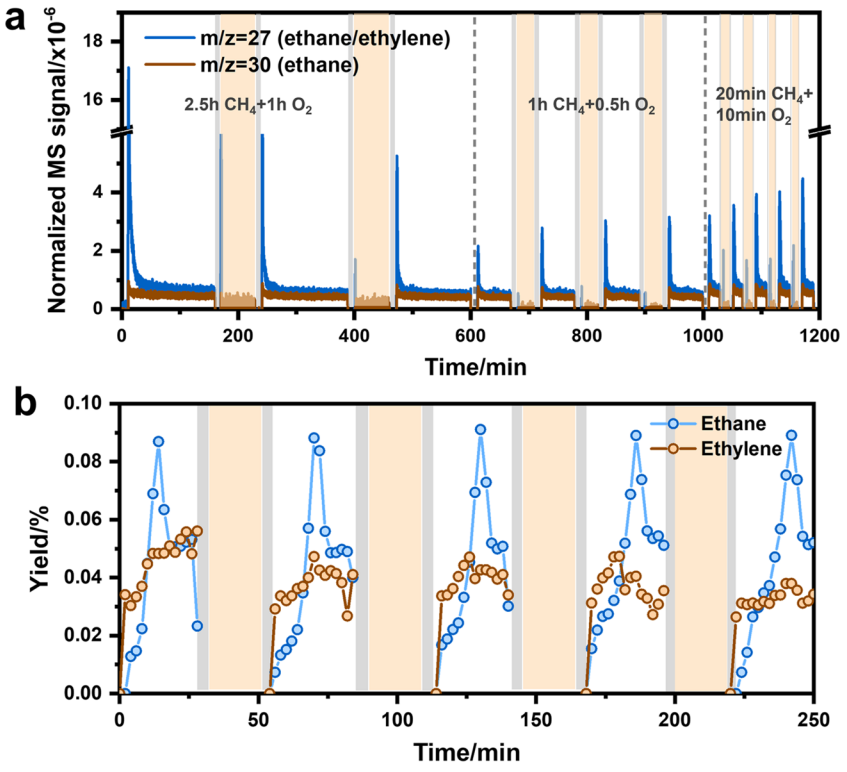

Figure 2. (a) Reaction−regeneration tests of the Pt/CeO_2 catalyst at 800 °C using 100 mg catalysts. A flow of 50 mL/min of He was purged to the reactor for 10 min between the NOCM reaction in 10 mL/min of 95 vol % CH_4 and the regeneration under 40 vol % O_2. (b) The ethane and ethylene yield obtained by GC during the reaction−regeneration cycles using 100 mg of Pt/CeO_2 catalyst at 800 °C. A total flow of 10 mL/min (95 vol % CH_4 + 5 vol % Ar for reaction and 40 vol % O_2 diluted by He for regeneration) was used for the measurements. The frequency of GC injection is every 2 min. The gray zone indicates the He purging, and the orange zone represents the regeneration treatment in O_2.

a Pt feature in terms of isolated Pt^{2+} ions in a square planar configuration in the CeO_2 surface.[15−18] The main products of the NOCM reaction with the Pt/CeO_2 catalyst at a reaction temperature of 800 °C were ethylene and ethane (Figure 1b). At the given conditions, ethane is obtained in larger amounts than ethylene. Coke was also formed on the Pt/CeO_2 catalyst (Figure S3). During the initial stage of reaction, the methane conversion decreases from ∼1% to ∼0.2%, which goes together

https://doi.org/10.1021/acs.jpclett.3c01179
J. Phys. Chem. Lett. 2023, 14, 6778−6783

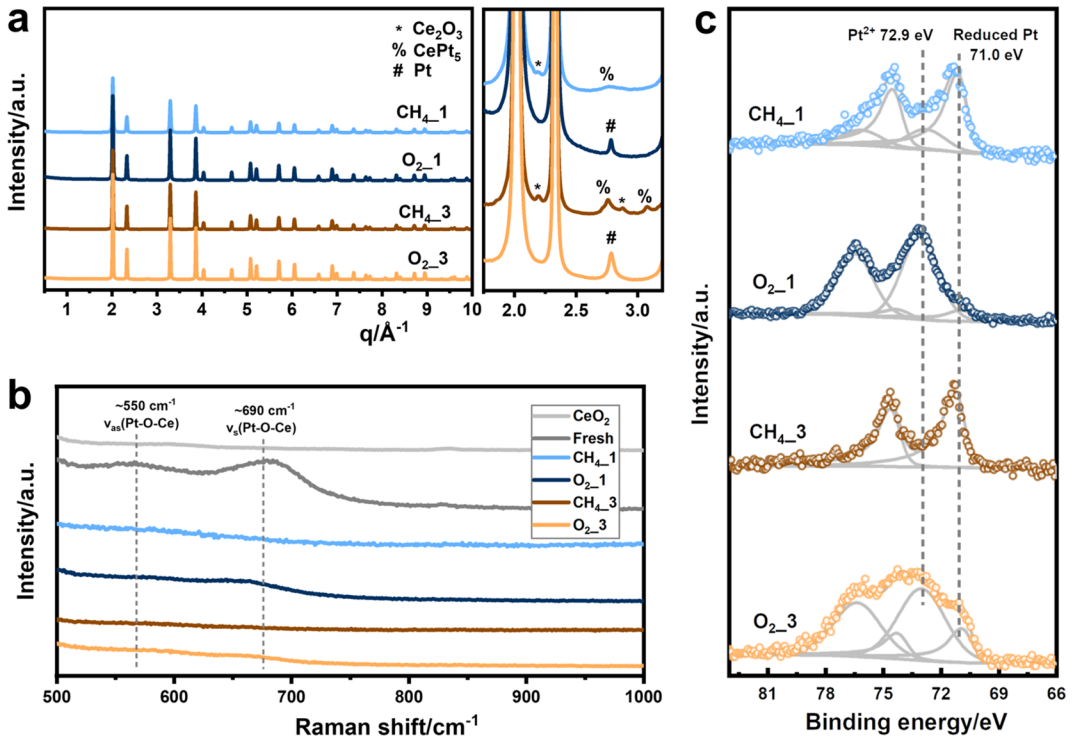

Figure 3. (a) Quasi *in situ* synchrotron XRD patterns with the enlarged region. (b) Raman spectra measured using the 532 nm laser. (c) Pt 4f XPS results of Pt/CeO_2 catalysts at different reaction/regeneration stages. In CH_4_n and O_2_n, "n" refers to the nth reaction or regeneration. CH_4_1 indicates the catalyst obtained after the first reaction stage, and the corresponding O_2_1 suggests the regenerated CH_4_1 sample after the O_2 treatment.

with a slow increase of the ethane and ethylene yield. The Pt/CeO_2 catalyst exhibits a C_2-hydrocarbon selectivity of 68% at a methane conversion rate of 0.85 $mmol_{CH4}$ g_{Pt}^{-1} min^{-1}, which is comparable with earlier reported activity data for Pt/CeO_2 tested under similar reaction conditions, namely, a C_2-hydrocarbon selectivity of 55% at a reaction rate of 0.34 $mmol_{CH4}$ g_{Pt}^{-1} min^{-1} at 780 °C.[8] The reaction involves an induction period, which is probably caused by the transformation of the initially isolated Pt^{2+} species. We characterized in detail the fresh and used Pt/CeO_2 catalysts. The synchrotron XRD pattern of fresh Pt/CeO_2 is dominated by diffraction lines from CeO_2 (PDF no. 00-004-0593). The pattern of the used sample contains additional features due to Ce_2O_3 (PDF no. 01-083-5456) and $CePt_5$ alloy (PDF no. 01-071-7052, Figure 1c, Figure S4). Diffraction peaks of Pt metal (PDF no. 00-004-0802) were not observed. The formation of $CePt_5$ in a Pt/CeO_2 sample reduced at high temperature in H_2 or CH_4 has been reported before.[11,19] Rietveld refinement points to the sintering of CeO_2 particles during the NOCM reaction (Figure S5 and Table S1), which is confirmed by TEM (Figure S6). The formation of $CePt_5$ is in line with XANES and EXAFS analysis (Figure 1a, Figures S1, S7, and S8, and Table S2). The reduction of Pt is also in keeping with the absence of Pt^{2+} in the XPS result of the used catalyst (Figure S2). Therefore, we can conclude that Pt on the catalyst surface was fully reduced into $CePt_5$. As such, it can be stated that the $CePt_5$ alloy is the active phase during a prolonged NOCM reaction, although the role of the initially present atomically dispersed Pt^{2+} sites needs to be further investigated.

We developed an oxidative regeneration strategy based on the work of Datye and co-workers. They reported that gaseous PtO_2 can be trapped by CeO_2, leading to isolated Pt species.[20] We employed an *in situ* O_2 regeneration at high temperature, consisting of periodically switching between a CH_4-containing reaction feed and an O_2-containing regeneration feed, aiming at the redispersion of agglomerated Pt. The evolution of the MS signals of 27 (ethylene and ethane) and 30 (ethane) in Figure 2a during consecutive reaction−regeneration cycles indicates the rapid decline of the C_2-hydrocarbon yield after the initial period (i.e., the m/z = 27 signal drops by 1 order of magnitude). This deactivation is likely caused by the rapid sintering of Pt in Pt/CeO_2. By optimizing the length of the reaction and regeneration treatments, we found that a regeneration period of 10 min in O_2 can already restore the initial catalytic activity. Nevertheless, the reaction−regeneration cycles lead to a decrease of the maximum C_2-hydrocarbon signals at m/z = 27 by nearly an order of magnitude after 4 cycles (Figure 2a). The higher formation rate of C_2-hydrocarbons upon regeneration was confirmed by GC analysis (Figure 2b). Other products including H_2, H_2O, and CO_2 and small amounts of benzene and toluene were also detected (Figure S9). To confirm the pivotal role of Pt, we also studied the reaction−regeneration cycles for CeO_2. Without Pt, the C_2-hydrocarbon signal at m/z = 27 is about 3 times lower in the first reaction cycle (Figure S10). The hydrocarbon products obtained with the bare CeO_2 support are likely due to homogeneous gas-phase reactions. Nevertheless, we cannot completely rule out the catalytic role of CeO_2 in methane activation. Chang and co-workers reported the reduced CeO_2 surface to be active in the NOCM reaction. Based on theoretical modeling, they proposed that frustrated Lewis pairs, involving surface Ce cations and oxygen vacancies, are candidate active sites for methane activation.[21] Nevertheless, the catalytic activity is substantially enhanced when Pt is

https://doi.org/10.1021/acs.jpclett.3c01179
J. Phys. Chem. Lett. 2023, 14, 6778−6783

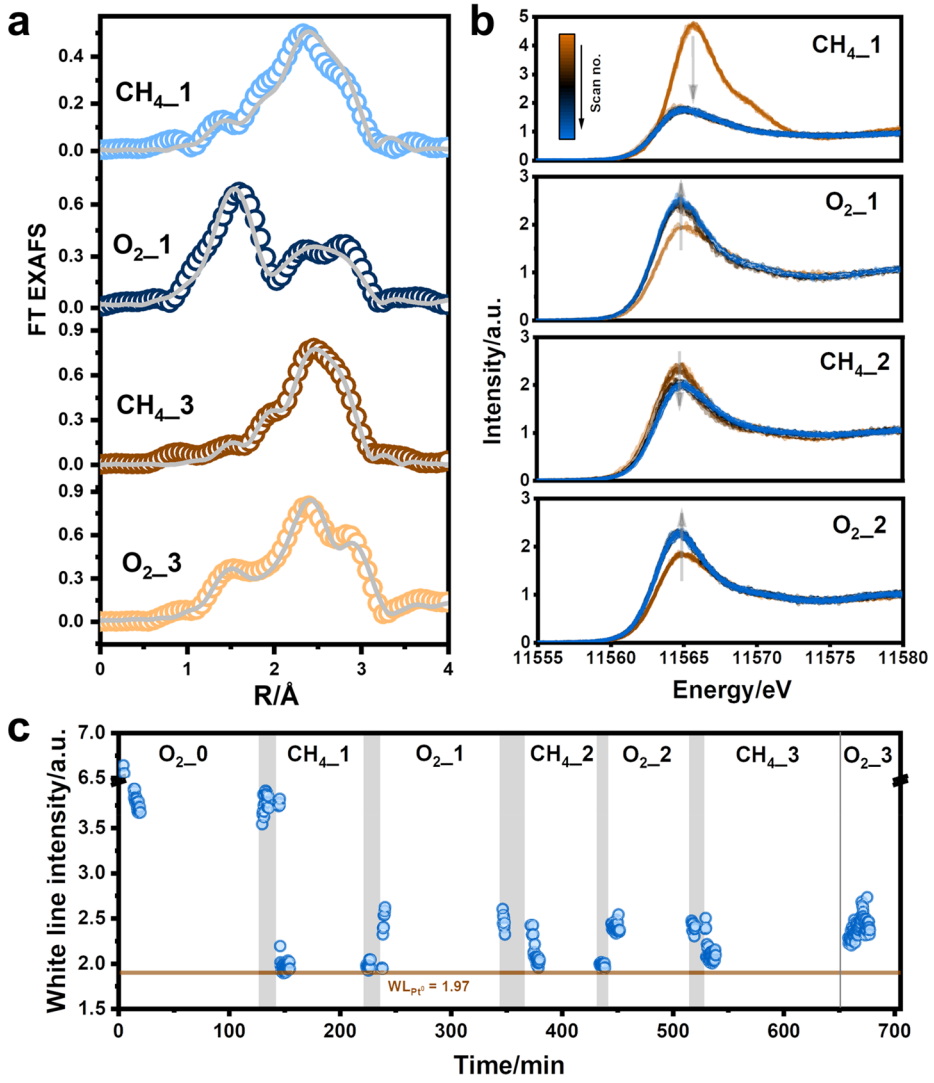

Figure 4. (a) Quasi *in situ* k^2-weighted EXAFS at the Pt L_3-edge of the Pt/CeO_2 catalyst at different reaction and regeneration stages. The raw data are shown using open circles, and the gray lines indicate the fitting results. (b) Pt L_3-edge HERFD-XANES spectra of the Pt/CeO_2 catalyst at different reaction and regeneration stages. (c) The evolution of white line intensity during the *in situ* HERFD-XANES measurements at the Pt L_3-edge. The measurements were performed at 800 °C using 30 mg of Pt/CeO_2 catalysts under 5 mL/min CH_4 for reaction and 15 mL/min 40 vol % of O_2 for regeneration. A flow of 20 mL/min of He was purged to the *in situ* cell between the NOCM reaction and the catalyst regeneration. The position of the white line intensity of Pt^0 is labeled. The He-purging period is labeled in gray.

introduced, showing that Pt plays an important role in the catalytic activity of Pt/CeO_2 catalysts. This conclusion is also in line with other studies of the role of Pt in Pt/CeO_2 for the NOCM reaction.[7,11]

The Pt/CeO_2 sample was characterized in detail after each reaction and regeneration cycle. The formation of Ce_2O_3 upon an NOCM cycle follows from the XRD patterns of CH_4_1 and CH_4_3 (in CH_4_n, "n" refers to the nth reaction cycle) and is likely caused by the reduction of CeO_2 by CH_4. However, the main phase present in the used materials is CeO_2. Ce_2O_3 was oxidized during regeneration as follows from the XRD patterns of the corresponding regenerated catalysts O_2_1 and O_2_3 (Figure 3a, in O_2_n, "n" refers to the nth regeneration cycle). With respect to Pt, the diffraction line at ~2.79 $Å^{-1}$ can be linked to the Pt metal in the O_2_1 and the O_2_3 samples. Upon reaction in CH_4, diffraction lines of $CePt_5$ are observed. Rietveld refinement of the synchrotron XRD patterns indicates the sintering of CeO_2 from ~7 to ~120 nm during the three reaction−regeneration cycles. The sintering of CeO_2 slowed after the third reaction stage. Meanwhile, the crystallite size of the $CePt_5$ particles increased from ~4 to ~8 nm, while the Pt^0 species observed after the oxidative regeneration have a size of ~20 nm (Table S1 and Figure S5). We further studied these samples by Raman spectroscopy (Figure 3b). The Raman bands at ~550 and ~690 cm^{-1}, which can be clearly observed in the fresh Pt/CeO_2 catalyst, are due to the asymmetric and symmetric stretching modes of the Pt−O−Ce moiety, respectively.[22] These two bands are not present anymore after the NOCM reaction but reappeared upon regeneration in O_2 albeit with a weaker intensity. The Raman results can be explained by the aggregation of Pt during the NOCM reaction and, subsequent, Pt redispersion during regeneration in the presence of O_2. XPS analysis reveals that 75% of surface Pt species are present in the reduced state after the first reaction cycle with the remaining 25% in the Pt^{2+} state. The fraction of Pt^{2+} increased to 88% after O_2 regeneration, pointing to redispersion of Pt on the catalyst surface (Figure 3c and Table S3). TEM analysis of Pt/CeO_2 catalysts also suggests the

https://doi.org/10.1021/acs.jpclett.3c01179
J. Phys. Chem. Lett. 2023, 14, 6778−6783

agglomeration and partial redispersion of Pt species upon CH_4 and O_2 treatments (Figure S11).

Quasi *in situ* EXAFS analysis was carried out to follow the changes in the Pt phase (Figures S12 and S13). The Pt−O coordination shell at ∼1.6 Å disappeared after the NOCM reaction in CH_4. However, this shell can be seen again after O_2 regeneration. There is also a second shell in the EXAFS after CH_4 or O_2 treatment, which can be linked to the formation of $CePt_5$ and/or Pt^0 particles based on the above-discussed synchrotron XRD data. As the second shell after the regeneration in O_2 cannot be assigned to bulk PtO_2 or PtO particles based on reference compounds, the presence of a Pt−O shell can be related to the partial redispersion of sintered Pt (Figure S12). EXAFS fitting shows that the coordination number of the Pt−O shell decreased from ∼3.8 to ∼0.4 during the first NOCM reaction and increased again to ∼2.8 during the first O_2 regeneration step. The coordination number of the Pt−O shell obtained after the third O_2 regeneration was lower at a value of ∼1, indicating a lower extent of redispersion (Figure 4a, Figure S14, and Table S4). Based on the above analysis, we infer that the enhanced catalytic performance of the Pt/CeO_2 catalyst after O_2 regeneration is caused by the reappearance of isolated Pt centers.

According to XPS and EXAFS, the reoxidation of reduced Pt to Pt^{2+} occurs during the redispersion of the sintered Pt species. Therefore, the redispersion of Pt can be tracked by following the oxidation state of Pt via the white line intensity of the Pt L_3-edge (Figure S15).[23] For this purpose, we carried out *in situ* HERFD-XAS to confirm the Pt evolution under actual reaction conditions. HERFD-XANES can provide enhanced energy resolution compared with the conventional total fluorescence yield detection method, allowing better monitoring of the changes in the XANES region (Figure S16). A home-built high-temperature *in situ* XAS cell with quartz tube reactor was used for the HERFD-XANES experiments at 800 °C (Figures S17 and S18). The white line intensity recorded at the Pt L_3-edge was employed to investigate the evolution of Pt (Figure 4b,c).[23] Upon heating the fresh catalyst in 40 vol % of the O_2 to 800 °C, the white line intensity decreased, indicating the reduction of Pt (Figure S19). After switching to CH_4, Pt reduction proceeded, as revealed by the further decrease of the white line intensity. This reflects the sintering of Pt. The Pt species were reoxidized after exposure to O_2, which implies redispersion of Pt centers. We continued the reaction−regeneration experiments and observed the periodic reduction and oxidation of Pt in CH_4 and O_2, respectively (Figure 4c). We compared the HERFD-XANES spectra obtained after each reaction and regeneration stage with the spectra of Pt^0 and $CePt_5$. The HERFD-XANES after the NOCM reaction is closer to that of $CePt_5$, whereas the O_2 regeneration step induced the formation of Pt^0 (Figure S20). These findings are consistent with the synchrotron XRD results. To determine the structure of the Pt phase, we measured HERFD-EXAFS of the Pt/CeO_2 catalyst at different reaction and regeneration stages at room temperature (Figure S21). It is clear that an additional shell at ∼1.6 Å appears after the O_2 treatment, which can be ascribed to the Pt−O single scattering path. These *in situ* tests confirm the redispersion of Pt after the O_2 regeneration. We verified that X-ray beam damage of the samples was negligible during the *in situ* HERFD-XAS measurements (Figure S22).

To summarize, Pt/CeO_2 with isolated Pt sites was investigated as a catalyst for the methane nonoxidative coupling reaction. Sintering of the initially isolated Pt^{2+} sites in CeO_2 is inevitable, involving the reduction not only of Pt but also of part of Ce, leading to $CePt_5$ particles. This $CePt_5$ alloy acts as the active phase during the prolonged NOCM reaction. An *in situ* O_2 regeneration strategy was developed, in which the Pt-containing particles can partially redisperse. This work highlights the dynamic nature of the Pt species in Pt/CeO_2 during the NOCM reaction and oxidative regeneration.

■ ASSOCIATED CONTENT

Supporting Information

The Supporting Information is available free of charge at https://pubs.acs.org/doi/10.1021/acs.jpclett.3c01179.

Experimental details; EXAFS, XANES, Raman, and XPS results of fresh and used Pt/CeO_2 catalysts and the catalyst after different reaction or regeneration stages; crystal structure; Rietveld refinement results of synchrotron XRD patterns; TEM images of Pt/CeO_2 catalysts; the results of the switching experiments over CeO_2; EXAFS fitting results of Pt/CeO_2 catalysts; MS data; surface fraction data; the procedure, experimental setup, and results of *in situ* HERFD-XANES measurements (PDF)

■ AUTHOR INFORMATION

Corresponding Authors

Nikolay Kosinov − *Laboratory of Inorganic Materials and Catalysis, Department of Chemical Engineering and Chemistry, Eindhoven University of Technology, 5600 MB Eindhoven, The Netherlands;* orcid.org/0000-0001-8520-4886; Email: n.a.kosinov@tue.nl

Emiel J. M. Hensen − *Laboratory of Inorganic Materials and Catalysis, Department of Chemical Engineering and Chemistry, Eindhoven University of Technology, 5600 MB Eindhoven, The Netherlands;* orcid.org/0000-0002-9754-2417; Email: e.j.m.hensen@tue.nl

Authors

Hao Zhang − *Laboratory of Inorganic Materials and Catalysis, Department of Chemical Engineering and Chemistry, Eindhoven University of Technology, 5600 MB Eindhoven, The Netherlands*

Valery Muravev − *Laboratory of Inorganic Materials and Catalysis, Department of Chemical Engineering and Chemistry, Eindhoven University of Technology, 5600 MB Eindhoven, The Netherlands;* orcid.org/0000-0002-1357-1086

Liang Liu − *Laboratory of Inorganic Materials and Catalysis, Department of Chemical Engineering and Chemistry, Eindhoven University of Technology, 5600 MB Eindhoven, The Netherlands*

Anna Liutkova − *Laboratory of Inorganic Materials and Catalysis, Department of Chemical Engineering and Chemistry, Eindhoven University of Technology, 5600 MB Eindhoven, The Netherlands*

Jérôme F. M. Simons − *Laboratory of Inorganic Materials and Catalysis, Department of Chemical Engineering and Chemistry, Eindhoven University of Technology, 5600 MB Eindhoven, The Netherlands*

Blanka Detlefs − *European Synchrotron Radiation Facility, 38043 Grenoble, France*

Huaizhou Yang − *Laboratory of Inorganic Materials and Catalysis, Department of Chemical Engineering and*

https://doi.org/10.1021/acs.jpclett.3c01179
J. Phys. Chem. Lett. 2023, 14, 6778−6783

Chemistry, Eindhoven University of Technology, 5600 MB Eindhoven, The Netherlands; orcid.org/0000-0001-7489-0948

Complete contact information is available at: https://pubs.acs.org/10.1021/acs.jpclett.3c01179

Notes

The authors declare no competing financial interest.

■ ACKNOWLEDGMENTS

This work is supported by the Advanced Research Center for Chemical Building Blocks, which is cofounded and cofinanced by The Netherlands Organization for Scientific Research and The Netherlands Ministry of Economic Affairs. We acknowledge Dr. Carlo Marini for the assistance in using the CLÆSS beamline at ALBA Synchrotron under proposal no. 2022025616. We acknowledge the European Synchrotron Radiation Facility for provision of synchrotron radiation facilities and we would like to thank Dr. Marta Mirolo for assistance in using beamline ID31 under the proposal no. MA5228. We acknowledge Timothy Bohdan and Dr. Pieter Glatzel for their help in using beamline ID26 under the proposal no. MA5121. We acknowledge SOLEIL for provision of synchrotron radiation facilities related to the experiments at the ROCK beamline under project no. 20210495. We thank Dr. Stephanie Belin for the assistance at ROCK. The experiments performed at ROCK were supported by a public grant overseen by the French National Research Agency (ANR) as part of the "Investissements d'Avenir" program (reference: ANR-10-EQPX-45). Rim C. J. van de Poll is acknowledged for performing the TEM measurements. We acknowledge Adelheid M. Elemans-Mehring and Thijs H. T. Moerkens for the assistance in ICP-OES measurements. Bianca Ligt is acknowledged for the assistance in FSP synthesis.

■ REFERENCES

(1) Zhang, H.; Hensen, E. J. M.; Kosinov, N., Heterogeneous catalysts for the non-oxidative conversion of methane to aromatics and olefins. *Comprehensive Inorganic Chemistry III*, Third ed.; Elsevier: Amsterdam, 2023; Vol. *6*, pp 311−326.

(2) Kosinov, N.; Hensen, E. J. M. Reactivity, selectivity, and stability of zeolite-based catalysts for methane dehydroaromatization. *Adv. Mater.* **2020**, *32*, 2002565.

(3) Vollmer, I.; Yarulina, I.; Kapteijn, F.; Gascon, J. Progress in developing a structure-activity relationship for the direct aromatization of methane. *ChemCatChem.* **2019**, *11*, 39−52.

(4) Meng, X.; Cui, X.; Rajan, N. P.; Yu, L.; Deng, D.; Bao, X. Direct methane conversion under mild condition by thermo-, electro-, or photocatalysis. *Chem.* **2019**, *5*, 2296−2325.

(5) Guo, X.; Fang, G.; Li, G.; Ma, H.; Fan, H.; Yu, L.; Ma, C.; Wu, X.; Deng, D.; Wei, M.; Tan, D.; Si, R.; Zhang, S.; Li, J.; Sun, L.; Tang, Z.; Pan, X.; Bao, X. Direct, nonoxidative conversion of methane to ethylene, aromatics, and hydrogen. *Science* **2014**, *344*, 616−619.

(6) Schwach, P.; Pan, X.; Bao, X. Direct conversion of methane to value-added chemicals over heterogeneous catalysts: challenges and prospects. *Chem. Rev.* **2017**, *117*, 8497−8520.

(7) Xie, P.; Pu, T.; Nie, A.; Hwang, S.; Purdy, S. C.; Yu, W.; Su, D.; Miller, J. T.; Wang, C. Nanoceria-supported single-atom platinum catalysts for direct methane conversion. *ACS Catal.* **2018**, *8*, 4044−4048.

(8) Bajec, D.; Kostyniuk, A.; Pohar, A.; Likozar, B. Micro-kinetics of non-oxidative methane coupling to ethylene over Pt/CeO_2 catalyst. *Chem. Eng. J.* **2020**, *396*, 125182.

(9) Wen, J.-H.; Wang, G.-C. Methane non-oxidative direct conversion to C_2 hydrogenations over CeO_2-supported Pt catalysts:a DFT study. *J. Phys. Chem. C* **2020**, *124*, 13249−13262.

(10) Ban, T.; Yu, X.-Y.; Kang, H.-Z.; Huang, Z.-Q.; Li, J.; Chang, C.-R. Design of SA-FLP dual active sites for nonoxidative coupling of methane. *ACS Catal.* **2023**, *13*, 1299−1309.

(11) Eggart, D.; Huang, X.; Zimina, A.; Yang, J.; Pan, Y.; Pan, X.; Grunwaldt, J.-D. Operando XAS study of Pt-doped CeO_2 for the nonoxidative conversion of methane. *ACS Catal.* **2022**, *12*, 3897−3908.

(12) Yao, Y.; Huang, Z.; Xie, P.; Wu, L.; Ma, L.; Li, T.; Pang, Z.; Jiao, M.; Liang, Z.; Gao, J.; He, Y.; Kline, D. J.; Zachariah, M. R.; Wang, C.; Lu, J.; Wu, T.; Li, T.; Wang, C.; Shahbazian-Yassar, R.; Hu, L. High temperature shockwave stabilized single atoms. *Nat. Nanotechnol.* **2019**, *14*, 851−857.

(13) Ma, X.; Sun, K.; Liu, J.-X.; Li, W.-X.; Cai, X.; Su, H.-Y. Single Ru sites-embedded rutile TiO_2 catalyst for non-oxidative direct conversion of methane: a first-principles study. *J. Phys. Chem. C* **2019**, *123*, 14391−14397.

(14) Muravev, V.; Spezzati, G.; Su, Y.-Q.; Parastaev, A.; Chiang, F.-K.; Longo, A.; Escudero, C.; Kosinov, N.; Hensen, E. J. M. Interface dynamics of $Pd−CeO_2$ single-atom catalysts during CO oxidation. *Nat. Catal.* **2021**, *4*, 469−478.

(15) Neitzel, A.; Figueroba, A.; Lykhach, Y.; Skála, T.; Vorokhta, M.; Tsud, N.; Mehl, S.; Ševčíková, K.; Prince, K. C.; Neyman, K. M.; Matolín, V.; Libuda, J. Atomically dispersed Pd, Ni, and Pt species in ceria-based catalysts: principal differences in stability and reactivity. *J. Phys. Chem. C* **2016**, *120*, 9852−9862.

(16) Tovt, A.; Bagolini, L.; Dvořák, F.; Tran, N.-D.; Vorokhta, M.; Beranová, K.; Johánek, V.; Farnesi Camellone, M.; Skála, T.; Matolínová, I.; Mysliveček, J.; Fabris, S.; Matolín, V. Ultimate dispersion of metallic and ionic platinum on ceria. *J. Mater. Chem. A* **2019**, *7*, 13019−13028.

(17) Wan, W.; Geiger, J.; Berdunov, N.; Lopez Luna, M.; Chee, S. W.; Daelman, N.; López, N.; Shaikhutdinov, S.; Roldan Cuenya, B. Highly stable and reactive platinum single atoms on oxygen plasma-functionalized CeO_2 surfaces: nanostructuring and peroxo effects. *Angew. Chem., Int. Ed.* **2022**, *61*, e202112640.

(18) Dvořák, F.; Farnesi Camellone, M.; Tovt, A.; Tran, N.-D.; Negreiros, F. R.; Vorokhta, M.; Skála, T.; Matolínová, I.; Mysliveček, J.; Matolín, V.; Fabris, S. Creating single-atom Pt-ceria catalysts by surface step decoration. *Nat. Commun.* **2016**, *7*, 10801.

(19) Bernal, S.; Calvino, J. J.; Gatica, J. M.; Larese, C.; López-Cartes, C.; Pérez-Omil, J. A. Nanostructural evolution of a Pt/CeO_2 catalyst reduced at increasing temperatures (473−1223 K): a HREM study. *J. Catal.* **1997**, *169*, 510−515.

(20) Jones, J.; Xiong, H.; DeLaRiva, A. T.; Peterson, E. J.; Pham, H.; Challa, S. R.; Qi, G.; Oh, S.; Wiebenga, M. H.; Pereira Hernández, X. I.; Wang, Y.; Datye, A. K. Thermally stable single-atom platinum-on-ceria catalysts via atom trapping. *Science* **2016**, *353*, 150−154.

(21) Huang, Z.-Q.; Zhang, T.; Chang, C.-R.; Li, J. Dynamic frustrated lewis pairs on ceria for direct nonoxidative coupling of methane. *ACS Catal.* **2019**, *9*, 5523−5536.

(22) Brogan, M. S.; Dines, T. J.; Cairns, J. A. Raman spectroscopic study of the $Pt−CeO_2$ interaction in the $Pt/Al_2O_3−CeO_2$ catalyst. *J. Chem. Soc., Faraday Trans.* **1994**, *90*, 1461−1466.

(23) Yoshida, H.; Nonoyama, S.; Yazawa, Y.; Hattori, T. Quantitative determination of platinum oxidation state by XANES analysis. *Phys. Scr.* **2005**, *2005*, 813.